Variable Eddington Factor Acceleration of Mixed Finite Element/Linear Discontinuous Galerkin Source Iteration

Samuel S. Olivier, Jim E. Morel

Department of Nuclear Engineering
Texas A&M University
College Station, TX 77843

Abstract

Abstract goes here

Keywords

Running Head

Corresponding Author
Jim E. Morel, Phone: (979)845-6072, FAX: (979)845-6075, E-mail: *morel@tamu.edu.*

1 Introduction

The Variable Eddington Factor (VEF) method, also known as Quasi-Diffusion (QD), was one of the first nonlinear methods for accelerating source iterations in S_n calculations []. It is comparable in effectiveness to both linear and nonlinear forms of Diffusion-Synthetic Acceleration (DSA), but it offers much more flexibility than the DSA. Stability can only be guaranteed with DSA if the diffusion equation is differenced in a manner consistent with that of the S_n equations []. Modern S_n codes often use advanced discretization schemes such as discontinuous Galerkin (DG) since classic discretization schemes such as step and diamond are not suitable for radiative transfer calculations in the high-energy density laboratory physics (HEDLP) regime or coupled electron-photon calculations. Diffusion discretizations consistent with the DG S_n discretizations cannot actually be expressed in diffusion form, but rather must be expressed in first-order or P_1 form, and are much more difficult to solve than standard diffusion discretizations. Considerable effort has gone into the development of "partially consistent" diffusion discretizations that yield a stable DSA algorithm with some degree of degraded effectiveness, but such discretizations are also generally difficult to develop. A great advantage of the VEF method is that the drift-diffusion equation that accelerates the S_n source iterations can be discretized in any valid manner without concern for consistency with the S_n discretization. When the VEF drift-diffusion equation is discretized in a way that is "non-consistent," the S_n and VEF drift-diffusion solutions for the scalar flux do not necessarily become identical when the iterative process converges. However, they do become identical in the limit as the spatial mesh is refined, and the difference between the two solutions is proportional to the spatial truncation errors associated with the S_n and drift-diffusion discretizations. In general the order of accuracy of the S_n and VEF drift-diffusion solutions will be the lowest order accuracy of their respective indepen-

dent discretizations. Although the S_n solution obtained with such a "non-consistent" VEF method is not conservative, the VEF drift-diffusion solution is in fact conservative. This is particularly useful in multiphysics calculations where the low-order VEF equation can be coupled to the other physics components rather than the high-order S_n equations. Another advantage of the non-consistent approach is that even if the S_n spatial discretization scheme does not preserve the thick diffusion limit [], that limit will generally be preserved using the VEF method.

The purpose of this paper is to investigate the application of the VEF method with the 1-D S_n equations discretized with the lumped linear-discontinuous method (LLDG) and the drift-diffusion equation discretized using the constant-linear mixed finite-element method (MFEM). To our knowledge, this combination has not been previously investigated. Our motivation for this investigation is that MFEM methods are now being used for high-order hydrodynamics calculations at Lawrence Livermore National Laboratory []. A radiation transport method compatible with MFEM methods is clearly desirable for developing a MFEM radiation-hydrodynamics code. Such a code would combine thermal radiation transport with hydrodynamics. However, MFEM methods are inappropriate for the first-order form of the transport equation, and are problematic even for the even-parity form. []. Thus the use of the VEF method with a DG S_n discretization and a MFEM drift-diffusion discretization suggests itself. Here we define a VEF method that should exhibit second-order accuracy since both the transport and drift-diffusion discretizations are second-order accurate in isolation. In addition, our VEF method should preserve the thick diffusion limit [], which is essential for radiative transfer calculations in the HEDLP regime. We use the lumped rather than the standard LDG discretization because lumping yields a much more robust scheme, and robustness is essential for radiative transfer calculations in the HEDLP

regime. Because this is an initial study, we simplify the investigation by considering only one-group neutron transport rather than the full radiative transfer equations, which include a material temperature equation as well as the radiation transport equation. The vast majority of relevant properties of a VEF method for radiative transfer can be tested with an analogous method for one-group neutron transport. Furthermore, a high-order DG-MFEM VEF method could be of interest for neutronics in addition to radiative transfer calculations. A full investigation for radiative transfer calculations will be carried out in a future study.

The remainder of this paper is organized as follows. First, we describe the VEF method analytically. Then we describe our discretized S_n equations, followed by a description of the discretized VEF drift-diffusion equation. We next give computational results. More specifically, we describe two ways to represent the S_n variable Eddington factor in the MFEM drift-diffusion equation and several ways to construct the S_n scattering source from the drift-diffusion solution for the scalar flux. Each of these options yields a different VEF method. The accuracy of these methods is then compared to that of the standard lumped LDG S_n solution for several test problems, and the iterative convergence rate of these methods is compared to that of the lumped LDG S_n equations with fully-consistent S_2 Synthetic Acceleration (S_2SA). Finally, we give conclusions and recommendations for future work.

2 The VEF Method

2.1 The Algorithm

Here, we describe the VEF method for a planar geometry fixed-source problem:

$$\mu \frac{\partial \psi}{\partial x}(x,\mu) + \sigma_t(x)\psi(x,\mu) = \frac{\sigma_s(x)}{2}\int_{-1}^{1} \psi(x,\mu')\,\mathrm{d}\mu' + \frac{Q(x)}{2}\,, \tag{1}$$

where $\mu = \cos\theta$ is the cosine of the angle of flight θ relative to the x–axis, $\sigma_t(x)$ and $\sigma_s(x)$ the total and scattering macroscopic cross sections, $Q(x)$ the isotropic fixed-source and $\psi(x,\mu)$ the angular flux. Applying the Discrete Ordinates (S_N) angular discretization yields the following set of N coupled, ordinary differential equations:

$$\mu_n \frac{\mathrm{d}\psi_n}{\mathrm{d}x}(x) + \sigma_t(x)\psi_n(x) = \frac{\sigma_s(x)}{2}\phi(x) + \frac{Q(x)}{2}\,, 1 \leq n \leq N\,, \tag{2}$$

where $\psi_n(x) = \psi(x,\mu_n)$ is the angular flux in direction μ_n. The μ_n are stipulated by an N-point Gauss quadrature rule such that the scalar flux, $\phi(x)$, can be numerically integrated with:

$$\phi(x) = \sum_{n=1}^{N} w_n \psi_n(x) \tag{3}$$

where the w_n are the quadrature weights corresponding to the μ_n.

The VEF method decouples Eq. 2 by lagging the scattering term:

$$\mu_n \frac{\mathrm{d}\psi_n^{\ell+1/2}}{\mathrm{d}x}(x) + \sigma_t(x)\psi_n^{\ell+1/2}(x) = \frac{\sigma_s(x)}{2}\phi^{\ell}(x) + \frac{Q(x)}{2}\,, 1 \leq n \leq N\,, \tag{4}$$

where the superscripts indicate the iteration index. In Source Iteration, the update

$$\phi(x)^{\ell+1} = \phi(x)^{\ell+1/2} \tag{5}$$

is used. However, this is slow to converge in optically thick and highly scattering systems. Instead, the VEF method solves the VEF drift diffusion equations found by taking the first two moments of Eq. 2:

$$\frac{\mathrm{d}}{\mathrm{d}x}J^{\ell+1}(x) + \sigma_a(x)\phi^{\ell+1}(x) = Q(x)\,, \tag{6a}$$

$$\frac{\mathrm{d}}{\mathrm{d}x}\langle\mu^2\rangle^{\ell+1/2}(x)\phi^{\ell+1}(x) + \sigma_t(x)J^{\ell+1}(x) = 0\,, \tag{6b}$$

where $J^{\ell+1}(x)$ is the current and

$$\langle\mu^2\rangle^{\ell+1/2}(x) = \frac{\int_{-1}^{1}\mu^2\psi^{\ell+1/2}(x,\mu)\,\mathrm{d}\mu}{\int_{-1}^{1}\psi^{\ell+1/2}(x,\mu)\,\mathrm{d}\mu} \xrightarrow{\mathrm{S}_N} \frac{\sum_{n=1}^{N}\mu_n^2\psi_n^{\ell+1/2}(x)w_n}{\sum_{n=1}^{N}\psi_n^{\ell+1/2}(x)w_n} \tag{7}$$

the Eddington factor. The scattering term in Eq. 4 is then updated with the VEF drift diffusion scalar flux found by solving Eqs. 6a and 6b. This process of solving Eq. 4 for the $\psi_n(x)$, computing the Eddington factor, solving the VEF drift diffusion equation for the scalar flux, and updating the scattering term with the VEF drift diffusion scalar flux is repeated until

$$\frac{\|\phi^{\ell+1} - \phi^{\ell}\|}{\|\phi^{\ell+1}\|} < \epsilon\,, \tag{8}$$

where ϵ is a sufficiently small tolerance.

Acceleration occurs because the angular shape of the angular flux, and thus the Eddington factor, converges much faster than the scalar flux. In addition, the VEF equations model the contributions of all scattering events at once, reducing the dependence on source iterations to introduce scattering information. The solution from the VEF equations is then an approximation for the full flux and not the $\ell - 1$ collided flux as it was without acceleration.

In addition to acceleration, this scheme allows the S_N equations and drift diffusion equations to be solved with arbitrarily different spatial discretization methods. The following sections present the application of the Lumped Linear Discontinuous Galerkin (LLDG) spatial discretization to the S_N equations and the Mixed Finite Element Method (MFEM) to the VEF drift diffusion equations.

2.2 Lumped Linear Discontinuous Galerkin S_N

The LLDG discretization of Eq. 4 is:

$$\mu_n \left(\psi_{n,i}^{\ell+1/2} - \psi_{n,i-1/2}^{\ell+1/2}\right) + \frac{\Sigma_{t,i} h_i}{2} \psi_{n,i,L}^{\ell+1/2} = \frac{\Sigma_{s,i} h_i}{4} \phi_{i,L}^{\ell} + \frac{h_i}{4} Q_{i,L}\,, \tag{9a}$$

$$\mu_n \left(\psi_{n,i+1/2}^{\ell+1/2} - \psi_{n,i}^{\ell+1/2}\right) + \frac{\Sigma_{t,i} h_i}{2} \psi_{n,i,R}^{\ell+1/2} = \frac{\Sigma_{s,i} h_i}{4} \phi_{i,R}^{\ell} + \frac{h_i}{4} Q_{i,R}\,, \tag{9b}$$

where h_i, $\Sigma_{t,i}$, and $\Sigma_{s,i}$ are the cell width, total cross section and scattering cross section in cell i. The i, L and i, R subscripts indicate the the subscripted value is the left or right discontinuous edge value. The cell centered angular flux is the average of the left and right discontinuous edge fluxes:

$$\psi_{n,i}^{\ell+1/2} = \frac{1}{2}\left(\psi_{n,i,L}^{\ell+1/2} + \psi_{n,i,R}^{\ell+1/2}\right)\,, \tag{10}$$

and the cell edged angular fluxes are defined through upwinding:

$$\psi_{n,i-1/2}^{\ell+1/2} = \begin{cases} \psi_{n,i-1,R}^{\ell+1/2}\,, & \mu_n > 0 \\ \psi_{n,i,L}^{\ell+1/2}\,, & \mu_n < 0 \end{cases}\,, \tag{11a}$$

$$\psi_{n,i+1/2}^{\ell+1/2} = \begin{cases} \psi_{n,i,R}^{\ell+1/2}\,, & \mu_n > 0 \\ \psi_{n,i+1,L}^{\ell+1/2}\,, & \mu_n < 0 \end{cases}\,. \tag{11b}$$

Equations 9a, 9b, 10, 11a, and 11b can be combined and rewritten as

$$\begin{bmatrix} \mu_n + \Sigma_{t,i} h_i & \mu_n \\ -\mu_n & \Sigma_{t,i} + \mu_n \end{bmatrix} \begin{bmatrix} \psi_{n,i,L}^{\ell+1/2} \\ \psi_{n,i,R}^{\ell+1/2} \end{bmatrix} = \begin{bmatrix} \frac{\Sigma_{s,i} h_i}{2} \phi_{i,L}^{\ell} + \frac{h_i}{2} Q_{i,L} + 2\mu_n \psi_{n,i-1,R}^{\ell+1/2} \\ \frac{\Sigma_{s,i} h_i}{2} \phi_{i,R}^{\ell} + \frac{h_i}{2} Q_{i,R} \end{bmatrix}\,, \tag{12}$$

for sweeping from left to right ($\mu_n > 0$) and

$$\begin{bmatrix} -\mu_n + \Sigma_{t,i} h_i & \mu_n \\ -\mu_n & -\mu_n + \Sigma_{t,i} h_i \end{bmatrix} \begin{bmatrix} \psi_{n,i,L}^{\ell+1/2} \\ \psi_{n,i,R}^{\ell+1/2} \end{bmatrix} = \begin{bmatrix} \frac{\Sigma_{s,i} h_i}{2} \phi_{i,L}^{\ell} + \frac{h_i}{2} Q_{i,L} \\ \frac{\Sigma_{s,i} h_i}{2} \phi_{i,R}^{\ell} + \frac{h_i}{2} Q_{i,R} - 2\mu_n \psi_{n,i+1,L}^{\ell+1/2} \end{bmatrix}, \tag{13}$$

for sweeping from right to left ($\mu_n < 0$). The right hand sides of Eqs. 12 and 13 are known as the scalar flux from the previous iteration, the fixed source, and the angular flux entering from the previous cell are all known. By supplying the flux entering the left side of the first cell, the positive-angled solution can be propagated from left to right by solving Eq. 12. Similarly, supplying the incident flux on the right boundary allows the negative-angled solution to be propagated from right to left with Eq. 13.

2.3 Mixed Finite Element Method VEF Drift Diffusion

Applying the MFEM to Eqs. 6a and 6b and enforcing continuity of current yields:

$$-\frac{6}{\Sigma_{t,i} h_i} \langle \mu^2 \rangle_{i-1/2} \phi_{i-1/2} + \left(\frac{12}{\Sigma_{t,i} h_i} \langle \mu^2 \rangle_i + \Sigma_{a,i} h_i \right) \phi_i - \frac{6}{\Sigma_{t,i} h_i} \langle \mu^2 \rangle_{i+1/2} \phi_{i+1/2} = Q_i h_i \,, \tag{14a}$$

$$\begin{aligned} -\frac{2}{\Sigma_{t,i} h_i} \langle \mu^2 \rangle_{i-1/2} \phi_{i-1/2} + \frac{6}{\Sigma_{t,i} h_i} \langle \mu^2 \rangle_i \phi_i - 4 \left(\frac{1}{\Sigma_{t,i} h_i} + \frac{1}{\Sigma_{t,i+1} h_{i+1}} \right) \langle \mu^2 \rangle_{i+1/2} \phi_{i+1/2} \\ + \frac{6}{\Sigma_{t,i+1} h_{i+1}} \langle \mu^2 \rangle_{i+1} \phi_{i+1} - \frac{2}{\Sigma_{t,i+1} h_{i+1}} \langle \mu^2 \rangle_{i+3/2} \phi_{i+3/2} = 0 \,, \end{aligned} \tag{14b}$$

where the Eddington factor is evaluated at iteration $\ell + 1/2$ and the scalar flux at $\ell + 1$. Here, the Eddington factor has been assumed to be constant in each cell with discontinuous jumps at the edges. The simplest method of converting the Eddington factor from LLDG

to MFEM is to compute the Eddington factor using the cell centered and cell edge angular fluxes using Eqs. and 10, 11a, and 11b.

A more consistent way to transfer the Eddington factor is to represent the LLDG angular flux as a linear function using the MFEM basis functions:

$$\langle\mu^2\rangle_i(x) = \frac{\sum_{n=1}^{N}\mu_n^2\left[\psi_{n,i,L}B_{i,L}(x)+\psi_{n,i,R}B_{i,R}(x)\right]}{B_{i,L}(x)\sum_{n=1}^{N}w_n\psi_{n,i,L}+B_{i,R}(x)\sum_{n=1}^{N}w_n\psi_{n,i,R}} \tag{15}$$

where

$$B_{i,L}(x) = \begin{cases} \frac{x_{i+1/2}-x}{h_i}\,, & x\in[x_{i-1/2},x_{i+1/2}] \\ 0\,, & \text{otherwise} \end{cases} \tag{16}$$

and

$$B_{i,R}(x) = \begin{cases} \frac{x-x_{i-1/2}}{h_i}\,, & x\in[x_{i-1/2},x_{i+1/2}] \\ 0\,, & \text{otherwise} \end{cases}\,. \tag{17}$$

When MFEM is applied, the integral over cell i of Eq. 15 is approximated with 2 point Gauss quadrature. The cell centered Eddington factors used in Eq. 14 are then:

$$\langle\mu^2\rangle_i = \frac{1}{2}\left[\langle\mu^2\rangle_i(x_L)+\langle\mu^2\rangle_i(x_R)\right] \tag{18}$$

where

$$x_{L/R} = \frac{x_{i+1/2}-x_{i-1/2}}{2} \mp \frac{x_{i+1/2}+x_{i-1/2}}{2\sqrt{3}} \tag{19}$$

are the transformed quadrature points.

Transport consistent boundary conditions are applied through a modified Marshak boundary condition:

$$J(x) = B(x)\phi(x) \tag{20}$$

where

$$B(x) = \frac{\int_{-1}^{1} |\mu| \psi(x,\mu)\, \mathrm{d}\mu}{\int_{-1}^{1} \psi(x,\mu)\, \mathrm{d}\mu} \,. \tag{21}$$

Once the MFEM scalar flux has been found, the LLDG scattering term must be reconstructed. Two methods have been tested: no reconstruction and van Leer cell centered slope reconstruction. The no reconstruction method sets the LLDG discontinuous left and right scalar flux to the MFEM edge scalar flux:

$$\phi_{i,L/R} = \phi_{i\mp 1/2} \,, \tag{22}$$

where the left hand side is reconstructed LLDG flux used in the scattering term of Eq. 4 and the right hand side the MFEM drift diffusion flux. The van Leer cell centered reconstruction is:

$$\phi_{i,L/R} = \phi_i \mp \frac{1}{4} \xi_{\text{van Leer}} \left[(\phi_{i+1} - \phi_i) + (\phi_i - \phi_{i-1}) \right] \,, \tag{23}$$

where $\xi_{\text{van Leer}}$ is the van Leer is the slope limiter given in [].

3 Computational Results

Figure 1 shows the convergence criterion

$$\frac{\| f^{\ell+1} - f^{\ell} \|}{\| f^{\ell+1} \|} \tag{24}$$

as a function of unaccelerated iteration number for $f = \phi(x)$ and $f = \langle \mu^2 \rangle (x)$. The large drop in the convergence criterion between the first and second iterations supports the claim that the angular shape of the angular flux, and thus the Eddington factor, converges rapidly.

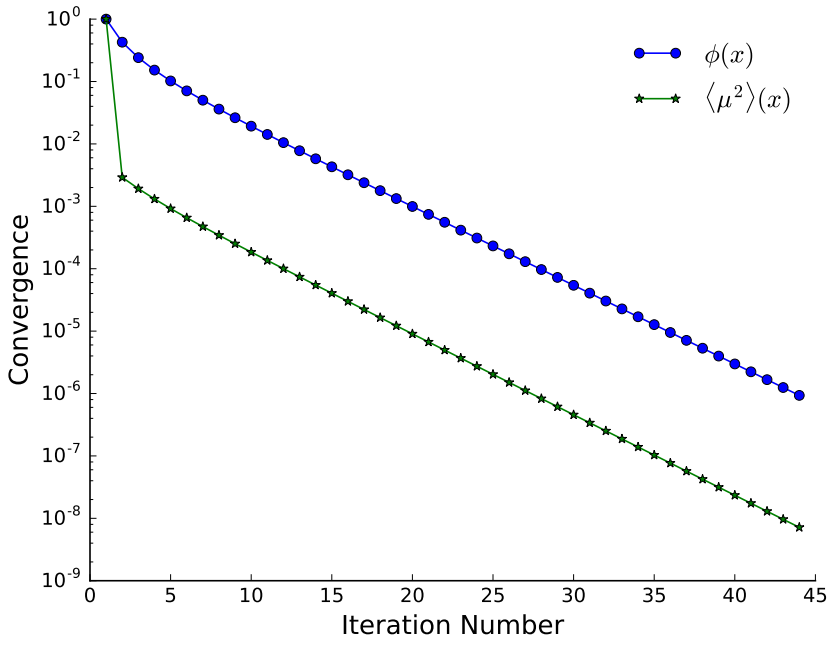

Figure 1: The convergence rate for $\phi(x)$ and $\langle\mu^2\rangle(x)$ for unaccelerated S_8 Source Iteration.

Reconstruction Method	ψ Representation	Order	C	R^2
None	Constant	1.997	0.682	9.9999×10^{-1}
None	Linear	1.998	0.687	1.0000
Center	Constant	2.007	0.726	9.9992×10^{-1}
Center	Linear	2.009	0.732	9.9991×10^{-1}

Table 1: The order of accuracy, error, and R^2 values for the permutations of the two Eddington representation methods and two slope reconstruction methods.

When compared to Fig. 2, a plot of the convergence criterion versus number of iterations for the VEF method, it is clear that the VEF method transfers the fast rate of convergence of the Eddington factor to the scalar flux.

Figure 3 compares Source Iteration, the VEF method, and consistently differenced S_2SA for varying ratios of σ_s to σ_t. The convergence tolerance was set to 1×10^{-10}. The VEF method performs similarly to S_2SA.

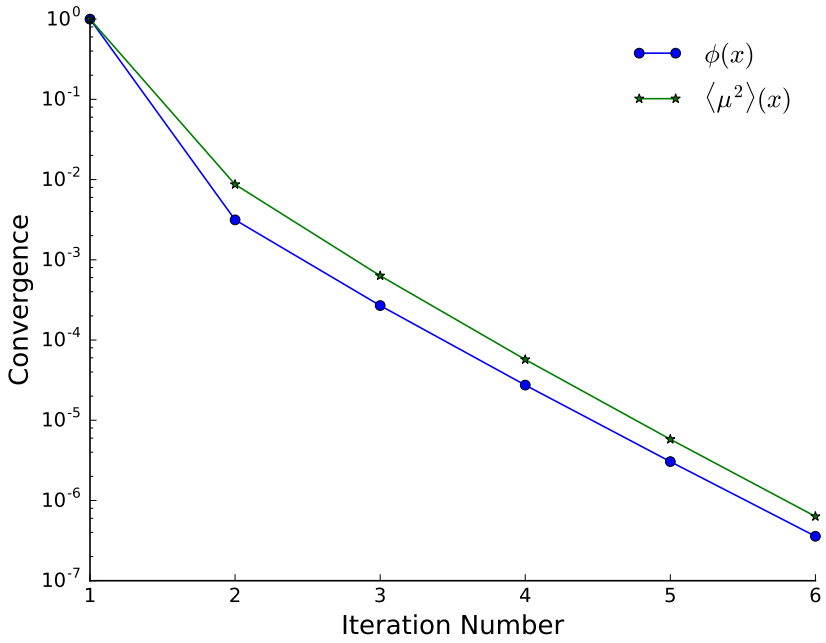

Figure 2: The convergence rate for $\phi(x)$ and $\langle \mu^2 \rangle(x)$ for VEF accelerated S_8.

4 Conclusions and Future Work

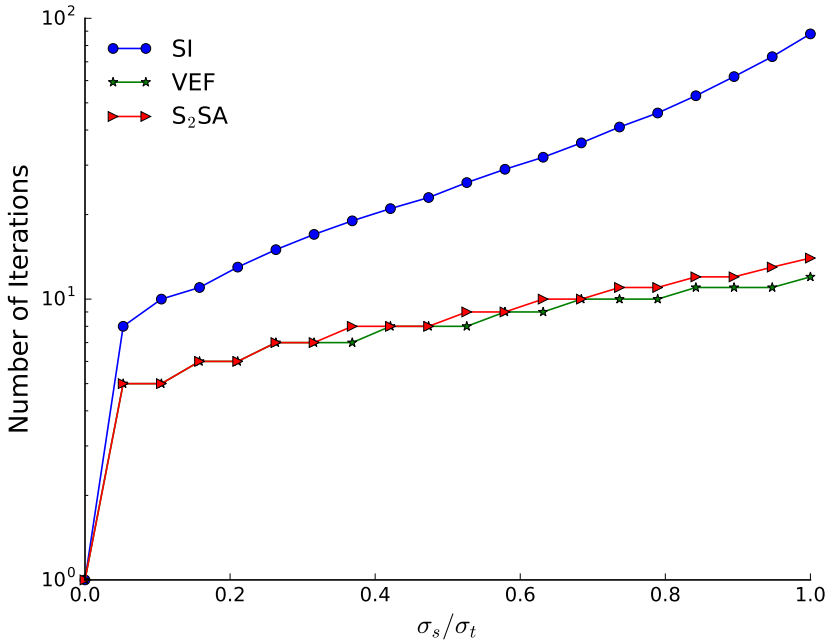

Figure 3: A comparison of the number of iterations required for Source Iteration, VEF acceleration, and S_2SA to converge for varying ratios of σ_s to σ_t.